chemosensors

MDPI

Review

Luminescent Sensors Based on the Assembly of Coinage Metal Nanoclusters

Chenyu Ren [1], Tong Shu [2,*], Xin Du [1], Linzhi Yang [2], Lei Su [2,*] and Xueji Zhang [2]

[1] Beijing Key Laboratory for Bioengineering and Sensing Technology, School of Chemistry and Biological Engineering, University of Science and Technology Beijing, Beijing 100083, China; chenyurenchenyu@163.com (C.R.); duxin@ustb.edu.cn (X.D.)

[2] School of Biomedical Engineering, Guangdong Laboratory of Artificial Intelligence and Digital Economy (SZ), Shenzhen Key Laboratory for Nano-Biosensing Technology, Research Center for Biosensor and Nanotheranostic, International Health Science Innovation Center, Health Science Center, Shenzhen University, Shenzhen 518060, China; yanglingzhi@szu.edu.cn (L.Y.); zhangxueji@szu.edu.cn (X.Z.)

* Correspondence: shutong@szu.edu.cn (T.S.); sulei@szu.edu.cn (L.S.)

Abstract: Coinage metals, such as Cu, Ag and Au, can form nanoclusters, which, when functionalized with ligands, have unique electronic and optical properties and are widely used in biomedical imaging, remote sensing, labeling, catalytic, etc. The mechanisms, structures and properties of nanocluster assemblies have been well reviewed. However, the collections and analyses of nanocluster assemblies for sensor application are few. This review examines different nanocluster sensor platforms with a focus on the assembly and analysis of the assembly processes and examples of applications.

Keywords: sensors; assembly; metal nanoclusters; supramolecular interactions

check for updates

Citation: Ren, C.; Shu, T.; Du, X.; Yang, L.; Su, L.; Zhang, X. Luminescent Sensors Based on the Assembly of Coinage Metal Nanoclusters. *Chemosensors* **2022**, *10*, 253. https://doi.org/10.3390/chemosensors10070253

Academic Editor: Ilaria Rea

Received: 11 May 2022
Accepted: 27 June 2022
Published: 30 June 2022

Publisher's Note: MDPI stays neutral with regard to jurisdictional claims in published maps and institutional affiliations.

Copyright: © 2022 by the authors. Licensee MDPI, Basel, Switzerland. This article is an open access article distributed under the terms and conditions of the Creative Commons Attribution (CC BY) license (https://creativecommons.org/licenses/by/4.0/).

1. Introduction

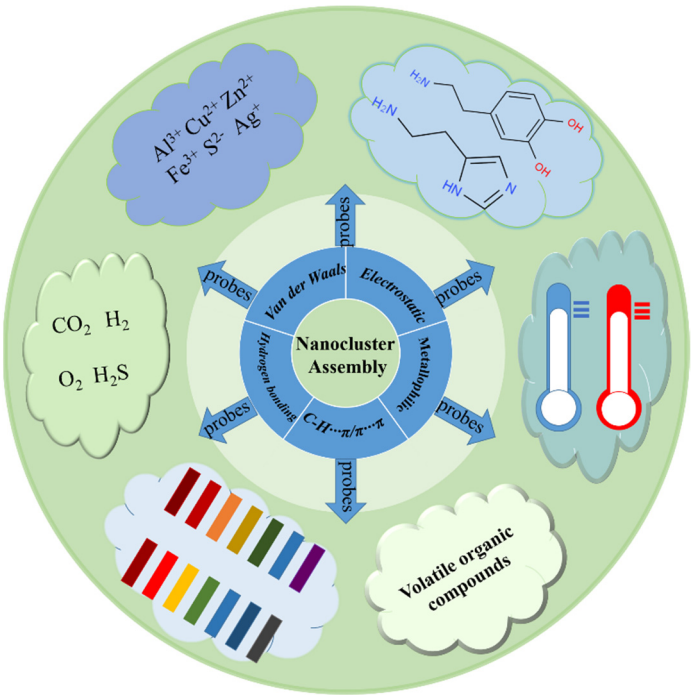
Metal nanoclusters (NCs) consist of several to a few hundred metal atoms, bridging the gap between small organometallic complexes and large metal nanoparticles (NPs) [1,2]. Coinage metal-based NCs, such as Cu, Ag and Au, have attracted extensive attention due to their unique electronic and optical properties and have been widely used in fields such as imaging [3], sensing [4], labeling [5] and catalysis [6,7]. The ultra-small sizes render the metal NCs with high surface energy and unstable in dispersed states. The attachment of ligands onto metal nanoclusters can effectively reduce the energy and stabilize the NCs with colloidal forms. So far, a wide variety of ligands have been developed for the fabrication of functional coinage metal NCs. One of the most used ligands in AuNCs fabrication is bovine serum albumin (BSA), which plays the roles of both reductant and end-capping reagent, and the resultant BSA-capped NCs can be used in imaged blood vessels and tumors in mice [8]. Polyethyleneimine protected AgNCs can be used to selectively detect Co^{2+} from 13 metal ions and image Hela cells [9], while cysteine-protected CuNCs with red emission are able to catalyze the degradation of toxic 4-nitrophenol to non-toxic 4-aminophenol [10]. Among these applications involving metal NCs, sensing technologies, which provide information on the composition of materials, have received much attention [11–13].

Sensing processes are usually composed of signal recognition, transduction and read-out [14,15]. The targets are recognized via the interaction with recognition components, and the ensuing signals are transduced and/or amplified into the forms that can be read out. Focusing on the luminescent sensor on the basis of metal NCs, common sensing mechanisms include aggregation-induced emission/quenching [16–18], ligand-induced charge transfer [19,20], fluorescence resonance energy transfer [21] and internal filtration effect [22]. Most of these optical sensors are constructed with colloidal metal NCs. However, these have limitations to their performances, particularly in relation to their stability during storage and deployment. Controllable aggregation of metal NCs as a whole might be an

effective way to enhance the sensing performances in certain applicable scenarios. For example, in the scenario of gas detection, aggregated metal NCs in a solid state are more feasible to interact with and then trap the targeted gas [23].

Assembly is an emerging topic in the field of metal NCs and mainly dominated by the ligands of metal NCs. Ligands on the clusters have different functional groups and can therefore be assembled with linking molecules or self-assembled through various supramolecular forces. The assembly of metal NCs bestows them with intriguing physicochemical properties beyond their dispersed status [24,25], such as assembly-induced emission enhancement [26–28], amplified light absorption and better mechanical strength [29]. Generally, metal NCs are assembled into topological nanomaterials with specific functions through supramolecular interactions, including the van der Waals interaction [30–32], hydrogen bond [33,34], electrostatic force [35–37], C-H···π/π···π [38–40] and metallophilic interactions [41–43]. Coinage metal NCs with the size of less than 2 nm and flexible modifiable ligand sites are regarded as excellent candidates for supramolecular building blocks [44,45]. The assembly orientates the structure of the NC aggregate by changing the spatial distribution of clusters, yielding a directional and stable spatial stacking structure [46]. The assembled metal NCs as the core can be well protected, and the resulting packed structures are conducive to charge/energy transfer, metal affinity interaction (Au, Ag and Cu) and photoelectric effects. Metal NCs assemblies possess desirable properties for the development of a new generation of sensors.

In this intriguing area, a variety of reviews have been published, but they mainly focused on the synthesis, structure and properties of metal NC assemblies. Reviews on luminescent sensors have rarely been investigated. As shown in Scheme 1, the assembly mechanisms of coinage metal NCs driven by several intermolecular forces are illustrated. Understanding the processes involved in the formation of the assemblies is essential for the development of a variety of sensor platforms. The understanding of metal NC assembly mechanisms provides the basis for the development of sensing technologies that can be used for the detection of organic compounds, inorganic ions, biomolecules and others. Finally, the current challenges of coinage metal NC assemblies are discussed, and their future opportunities can be envisaged.



Scheme 1. The schematic diagram shows the driving force and sensing applications of the assembly of NCs.

2. Assembly Mechanism of Coinage Metal NCs

Inspired by well-established nanoparticles self-assembly techniques, the assembly of coinage metal NCs can be effectively regulated by controlling the distribution and interaction of ligands on the surface of NCs. Therefore, regulating the interactions between ligands is an effective way to construct NCs with exotic structures. Next, we will classify and discuss the ligand interaction forces during cluster assembly.

2.1. Van der Waals Interaction

Van der Waals interaction between atoms and molecules plays an important role in chemistry, physics and materials science [47]. Although not strong, the accumulation of such interactions enables topological macromolecules, such as enzymes, proteins and DNA, to preserve their stable functional shape for biological activity. Similarly, Van der Waals interactions are also very important in initiating NCs in the long-range periodic assembly.

Van der Waals forces and dipole attraction can synergistically promote the assembly of NCs. For example, Yang et al. synthesized CuNCs using 1-dodecyl mercaptan (DT) as ligand to form independent banded structures in colloid solution [32]. The permanent dipole moment of $Cu_{12}DT_8AC_4$ was as high as 19.627 D. Driven by strong dipole attraction, CuNCs self-assembled into NWs in 1D orientation. The self-assembly structure was further strengthened by the van der Waals interaction attraction between DT molecules on CuNCs. The thickness of the strip could be adjusted to a single NCs scale by adjusting the dipole attraction between CuNCs and the van der Waals attraction between DT. Such independent bands showed excellent catalytic activity and durability in oxygen reduction reactions. In addition to simple two-dimensional structures, NCs could be assembled into spiral structures by the van der Waals interaction. Zhang et al. synthesized AuNCs assembly using $HAuCl_4 \cdot 4H_2O$ as the Au precursor, n-octadecanethiol as the reducing agent and ligand, liquid paraffin (LP) and benzyl ether (BE) as the solvent [30]. The assembly was a three-dimensional spiral nanostructure of several microns in length, hundreds of nanometers in width and tens of nanometers in thickness. In the process of assembly, the surfaces of the adjacent AuNCs ligands interacted with each other by the van der Waals force and produced the ligand overlap. The overlap of ligands generated rigidity instead of a certain degree of flexibility. Due to the poor solubility of AuNCs in the mixture of LP and BE, AuNCs formed irregular aggregates at room temperature. Different annealing temperatures and the ratio between LP and BE, which significantly affected the interactions within ligands, determined the final morphology of AuNCs assembly. Very recently, intriguing double-helix structures of NCs based on the van der Waals forces have been constructed. Zhu et al. successfully synthesized $Ag_{70}(TBBT)_{42}(TPP)_5$ by "$NaSbF_6$" mediated two-phase exchange method using 4-tert-butylbenzenethiol (TBBT) and triphenylphosphine (TPP) as ligands [31]. The NCs were self-layered and assembled into a complex secondary structure with a double-helix dense packing mode. The multiple van der Waals forces between molecules were the key factor for maintaining the stacking pattern of a double-helical 4H, which was also affected by the interlocking between the phosphine ligands of adjacent NCs. Complex DH4H stacking patterns could be transformed into simple 2H assembly by the alternations of surficial phosphine ligands. In another example, Jin et al. prepared a double-helix structure assembled by the heterodimeric $Au_{29}(SAdm)_{19}$, which contained four major motifs and perfectly balanced conformational matching (attraction) and steric repulsions [48]. This equilibrium was achieved through the van der Waals forces that drove the NCs to rotate in solution, so that the surface motifs were paired with the adjacent enantiomer NCs by appropriate anisotropic interactions (Figure 1).

2.2. Electrostatic Interactions

NCs can be assembled by electrostatic interactions between species with opposite charges, known as electrostatic attraction. Therefore, NCs can be assembled successfully by adding substances with opposite charges to the NCs. Counterions are often added to induce the formation of NC assemblies. For example, Wang et al. assembled $Ag_{29}(SSR)_{12}$ clusters

into one-dimensional cluster-based lines using the electrostatic attraction between Cs^+ ions and negatively charged $[Ag_{29}(SSR)_{12}]^{3-}$. Such assembly was further strengthened by the interaction between the Cs-S bond and Cs···π interactions [35]. The oppositely charged polymers can also be used to form the assembling structures with metal NCs. For example, Zang et al. synthesized $Au_{10}(C_{21}H_{27}O_2)_{10}$ by utilizing alkyne-modified levonorgestrel as a protective ligand and then assembled it with cationic polymer poly(allylamine hydrochloride) (PAH) (Au_{10}NC-PAH) to prepare an assembly with a size of about 100 nm [36]. Electrostatic interactions between PAH and the ligands on the surface of the Au clusters led to aggregation-induced emission with 4–6-fold fluorescence enhancement and the final quantum yield of 49.8%. In addition, compared with Au_{10}NCs, the Au_{10}NC-PAH assemblies had unique advantages in effectively realizing antibody-mediated actin imaging and drug release. Surfactants can similarly act as the counterions for the assembly of metal NCs and elevate the fluorescence intensity of metal NCs. For example, Hao et al. designed fluorescence-enhanced complexes using GSH-CuNCs and cetyltrimethylammonium cations (CTAX) [37], which opened up a new way for the application of light-emitting diodes (Figure 2). The assembly of GSH-CuNCs and CTAX by electrostatic interaction formed an amphiphilic complex, which could easily be modulated by electrostatic interactions between CTAX and the counterbalancing ions Br^-, Cl^- and $C_7H_8O_3S^-$. As the surfactant concentration increased, the morphologies of the complex changed from ordered nanoparticles to network structures. Companied with the level of the assembly, this assembly resulted in aggregation-induced emission phenomenon with enhanced fluorescence.

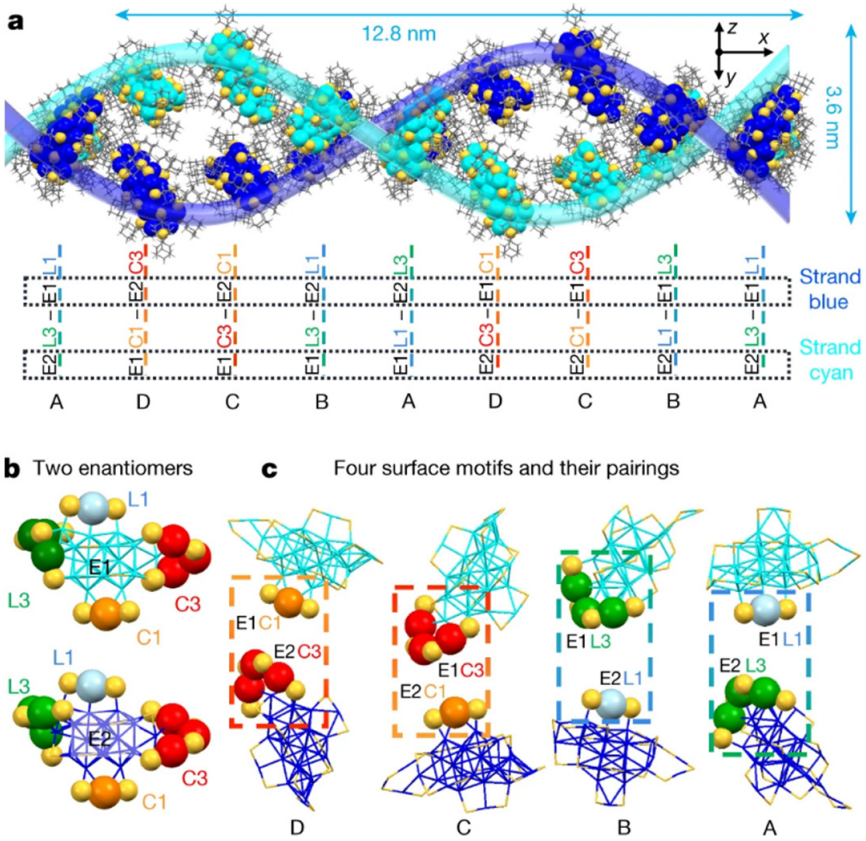


Figure 1. (**a**) Two enantiomers of $Au_{29}(SR)_{19}$ in supercrystal (E1 and E2); (**b**) The enantiomers contain four distinct major motifs, denoted as L1 and L3, C1 and C3; (**c**) Four types of motif matching between adjacent enantiomers in the supercrystal. Copyright 2021 Springer Nature.

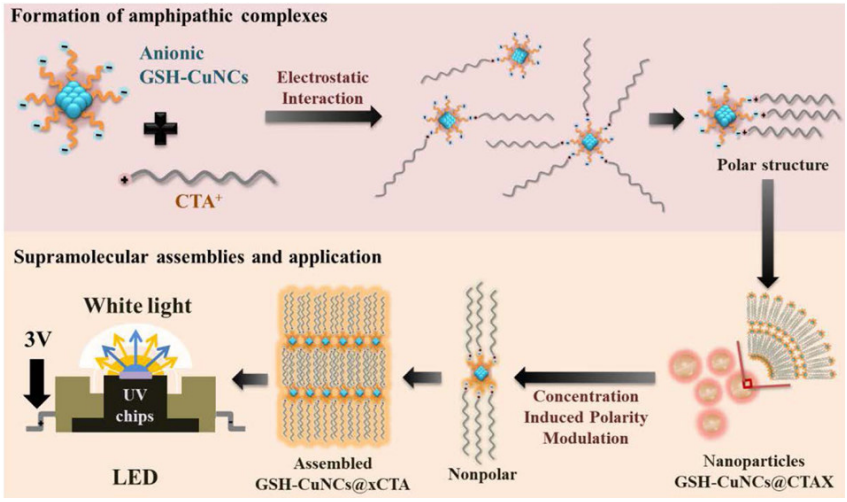


Figure 2. The stepwise assembly of the GSH-CuNCs composite used as a light-emitting diode. Copyright 2021 American Chemical Society.

2.3. Hydrogen Bonding Interactions

The essence of the hydrogen bond is the electrostatic force between hydrogen nucleus on the strong polar bond and the electronegative atom containing lone electron pair with partial negative charge. The preparation of several cluster-based stimuli-responsive materials is driven by hydrogen bonding. For example, Xie et al. prepared a novel water-soluble Ag_9NCs ($(NH_4)_9[Ag_9(MBA)_9]$) in order to study the effect of carboxyl groups in NCs on ligand positions during assembly [33]. When ethanol was added, the Ag_9NCs self-assembled into highly ordered fiber networks via hydrogen bonds in aqueous solution and further crosslinked into gels with structural rearrangement, leading to enhanced photoluminescence. Meanwhile, the addition of polar organic solvents induced conversion from fluorescence to phosphorescence. As the temperature increased, the shape could reversibly change from fiber to sphere. The gelation state and the corresponding emission intensity were simultaneously restored as the fiber state was re-established. This cycle could be performed at least five times. In addition to temperature, cluster assembly materials can also be used to respond to pH. Cui et al. constructed an $Au_{22}(SG)_{18}$ (SG, glutathione) assembly via hydrogen bonding to simulate capsid protein assembly [34]. By controlling the dynamic intermolecular forces among $Au_{22}(SG)_{18}$ clusters, the dispersed NCs could self-assemble into nano, medium and micro scale spherical superpolymers in a template-free manner in aqueous dimethyl sulphoxide binary solvent. Inspired by the peptide/protein engineering self-assembly, DMSO was added to the AuNCs solution to break the hydrogen bond between water and AuNCs, which otherwise promoted the hydrogen bond bonding within ligands of AuNCs (Figure 3). The decrease in solution pH values augmented the proportion of the protic carboxyl group in AuNC ligands, resulting in the increase in hydrogen bonds, the reduction in the electrostatic repulsion and the increase in AuNC size. Hydrogen bonding between GSH ligands could also be constructed by using water–DMSO or water–DMF binary solvent system for dialysis of AuNCs. Water–DMSO cosolvent had a higher dielectric constant than that of water–DMF cosolvent, thus more effectively shielding the repulsion between negatively charged AuNCs, resulting in larger assemblies.

2.4. C-H···π/π···π Interactions

The weak attraction between the C–H bond and the delocalized π electrons system is called the C–H···π interaction [49] and that between the delocalized π electrons is known as the π···π interaction. C–H···π/π···π interactions are essential in the crystal assembly of NCs. For example, AbdulHalim et al. synthesized tetravalent $Ag_{29}(BDT)_{12}(TPP)_4$ NCs using bidentate ligand, which was easily assembled to form a crystal with a definite

structure [38]. The self-assembled supramolecular structure of $[Ag_{29}(BDT)_{12}(TPP)_4]_3NC$ crystals driven by the C–H···π interaction was obtained by dispersive centrifugal NCs in DMF and dropping onto microscope slides to evaporate the solvent. In another example, Li et al. paired cations $[Au_{21}(SC_6H_{11})_{12}(DPPM)_2]^+$NCs ($HSC_6H_{11}$ = cyclohexanethiol) with different counterbalancing anions $[AgCl_2]^-$ and $[Cl]^-$ to form one-dimensional nanofibril assemblies [39]. The single crystal was formed by counteracting the interaction of anions with π···π, anions ···π, and aryl C-H·· Cl with benzene ligands, and subsequently diffusing non-solvent (pentane) into NCs (pentane: CH_2Cl_2 = 10:1 in volume) solution. Due to the configuration change caused by counteracting the π–π interaction between the anions and benzene rings of ligands, the clipping of related counter-ions significantly enhances the electrical transport properties of NC assemblies. Recently, Huang et al. synthesized chiral luminescent $[Ag_{30}(C_2B_{10}H_9S_3)_8(DPPM)_6]$ (Ag_{30}-RAC) using carboranetrithiolate and phosphine as protective ligands and hydrazine as the reducing agent [40]. The chiral properties of Ag_{30}-RAC were induced by the ligand helical arrangement guided by B–H···π and C–H···π bond interactions between carborane cages and benzene rings. The interaction between B-H···π, C-H···π, π···π and van der Waals directed the self-assembly of Ag_{30}-RAC into a spiral structure when Ag_{30}-RAC crystallized in dimethylacetamide, and the spontaneous separation of the racemates was realized (Figure 4).

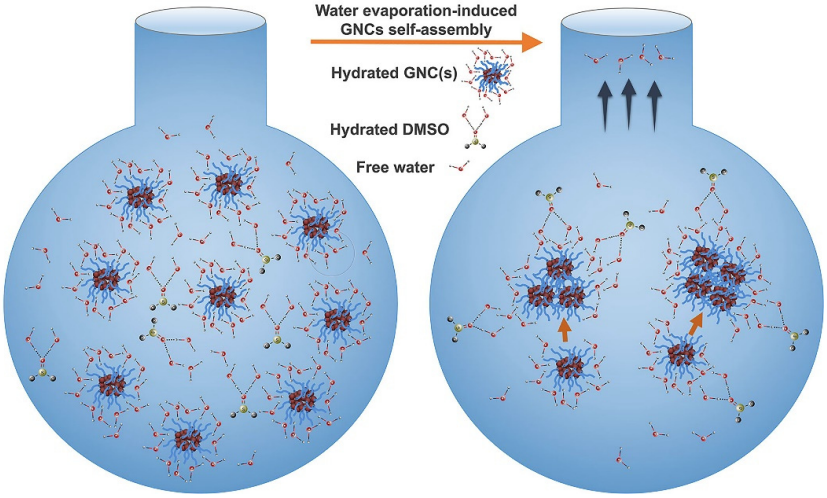


Figure 3. Schematic diagram of AuNCs self-assembly induced by dynamic water evaporation in water–DMSO binary solvents. Copyright 2018 American Chemical Society.

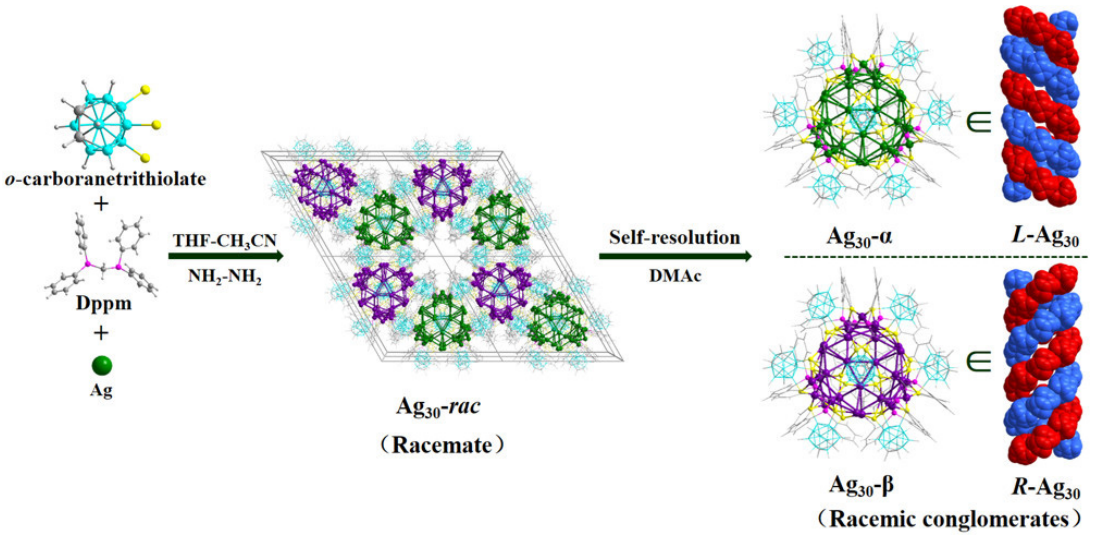


Figure 4. Synthesis and self-decomposition of Ag_{30}-RAC. Copyright 2020 American Chemical Society.

2.5. Metallophilic Interactions

Weak interactions between metal ions in closed shells are often referred to as metallophilic interactions [50]. Metallophilic interactions are important for the supramolecular self-assembly of precious metal clusters. The aurophilic interaction is often used to construct the assembly of precious metal NCs. For example, Xie et al. studied the aurophilic properties of $Au_{25}(SR)_{18}$ in the process of self-assembly into nanoribbons [41]. By adjusting the pH, $Au_{25}(SR)_{18}$ was transformed into a longer SR-[Au(I)-SR]$_x$ motif ($x > 2$) and a smaller Au^0 core. The reconstruction of NC surface motifs increased Au(I) content in the shell, facilitating the aurophilic interaction between adjacent NCs. The AuNCs were compact in nanoribbons with a quantum yield of 6.2%. In a similar example, Mandal et al. synthesized a 1D chain structure using $[Ag_4(S\text{-}Adm)_6]^{2-}$ (S-Adm = 1-adamantanethiol) as the basic unit and stabilized the chain through the argentophilic interaction between adjacent NCs [42]. Then, the hydrophobic interactions between adamantane molecules in adjacent chains generated a two-dimensional supramolecular structure. In another example, Yang et al. developed a self-assembly strategy that could significantly enhance the luminous intensity of DT-capped CuNCs (DT = 1-dodecanethiol) [43]. As shown in Figure 5, the migration rate of the DT alkyl chain on NCs was increased by annealing, which was beneficial to the 2D directional self-assembly of NCs by the van der Waals force. After assembly, the compact component promoted the cuprophilic interaction and inhibited the intramolecular vibration and rotation of the ligand, hence giving rise to the strong fluorescence. Interestingly, the annealing temperature was able to control the emission color and intensity of the NC units.

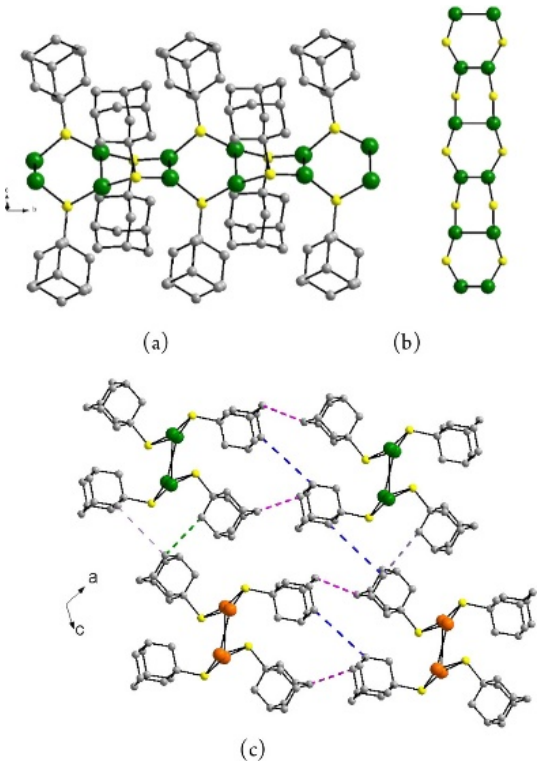


Figure 5. (**a**) One-dimensional Ag−S chain; (**b**) Ag−S connectivity creates a 6-membered ring; (**c**) One-dimensional chains are arranged in a two-dimensional supramolecular structure. Copyright 2015 American Chemical Society.

Summary of different methods used to demonstrate the assembly of NCs is given in Table 1.

Table 1. The assembly mechanism of coinage metal NCs.

Interactions	Strength of the Bonds (kJ/mol)	Nature	Advantages	Disadvantages	Application
Van der Waals interaction	2–20	The van der Waals forces are distance-dependent weak electrostatic attractions or repulsions that arise due to the fluctuating electromagnetic polarization of nearby atoms, molecules or particles.	The accumulation of Van der Waals interactions enables topological macromolecules to preserve their stable functional shape for biological activity. Van der Waals interactions are also very important for initiating NCs periodic assembly in the long range.	Van der Waals forces are not very strong.	Catalytic [32]. Detection [51].
Electrostatic force	20–40	Electrostatic interactions are generally strong attractions or repulsions between two oppositely charged ions, mostly positive and negative charges.	Electrostatic attraction has no direction, and the interaction between the anions and cations can be in any direction.	Self-assembly of two counter-charged NCs is difficult, owing to the instability of cationic NCs.	Imaging and drug delivery [36]. Light-emitting diodes [37]. Detection [17,21,52] Temperature [53], pH sensing [54,55]
Hydrogen bond	25–40	The essence of hydrogen bond is the electrostatic force between hydrogen nucleus on the strong polar bond and electronegative atom containing lone electron pair with partial negative charge.	Sophisticated networks of hydrogen bonds with flexible and structure-directing properties.	The conditions for forming the most stable hydrogen bonds are harsh.	Temperature sensing [33] pH sensing [34] Detection [56,57].
C-H···π/π···π	3-8/8–12	The weak attraction between the C–H bond and the delocalized π electrons system is called and that between the delocalized π electrons is known as π···π interaction.	The C–H···π interactions play an important role in the nanoscale assemblies and crystal packing of and were further extended to explain the crystallization of larger NCs.	The C–H···π attraction is often considered the weakest hydrogen bonding interaction occurring between the soft acids and bases.	Electrical Transport [39]. Separation of the racemates [40]. Detection [58].
Metallophilic interactions	25–30 (aurophilic interactions)	Weak interactions between metal ions in closed shells are often referred to as metallophilic interactions.	Metallophilic interactions are weak; they will be very prominent in the presence of particular solvents.	Metallophilic interactions are weak.	Light-emitting diodes [43]. Detection [59]. Temperature sensing [16,20]

3. Sensing Application

The assembled coinage metal NCs were efficiently used in the detection of organic compounds, inorganic ions, biomolecules and other analytes due to their aggregation-induced luminescence, stimuli responsiveness and reversibility. Next, we will carry out specific discussions according to the different analytical targets.

3.1. Metal Ions

With the continuous development of industry, various heavy metal ions are intentionally discharged or accidently leaked to the environment with the resulting exposure via food and accumulation in humans. A typical example is mercury, which is harmful to the environment and can affect the metabolism, immune and central nervous systems in

humans [60]. Therefore, there is a need to develop a sensitive, cheap, efficient, fast and environmentally friendly mercury sensor. Zhou et al. reported the preparation of AgNCs self-assembled particles with aggregation-induced emission [18]. AgNCs were prepared by a one-step method using thiosalicylic acid as the ligand. The hydrophobicity of thiosalicylic acid drove AgNCs to self-assemble into AgNCs self-assembled particles with bright red luminescence and selective response to mercury ions in aqueous solution. Only 4.0 mM of Hg^{2+} could completely quench the luminescence of AgNCs assembly, achieving high sensitivity and selective quantification of Hg^{2+}. Pandurangan et al. prepared assemblies of 2-mercaptobenzothiazole-protected AgNCs (SA-AgNCs) using the same strategy, which were directly caused by hydrophobicity and bridging-type coordination [61]. The obtained SA-AgNCs possessed orange luminescence, which could be quenched by the strong aurophilic interaction between Hg^{2+} and Ag^{+}. The SA-AgNCs could sensitively detect Hg (II) ions in the range of 3.5–100 nM, which had great potential in detecting Hg^{2+} ions in tap water and breast milk samples. Wang et al. prepared CuNCs using 4-chlorothiophenol as the ligand [51]. In neutral or alkaline water environments, CuNCs exhibited red fluorescence induced by self-assembly through the van der Waals forces and dipole gravity. An Hg–SR complex formed between Hg^{2+}, and the ligand covered the surface of the Cu core, resulting in fluorescence quenching of CuNCs. The detection limit was as low as 0.3 nM. In addition, the assembled CuNCs could be used to prepare novel fluorescent bands for rapid detection of Hg^{2+} content in environmental water samples.

Al^{3+} can cause neurodegeneration in the brain, memory loss and even Alzheimer's disease [62]. Xin et al. obtained enhanced luminescence AgNCs assembly using polyethylene imine (PEI) as the template through electrostatic interaction [63]. The coordination of Al^{3+} with N of PEI induced the collapse of Ag_6-NCs/PEI nanovesicles, leading to luminescence quenching. The detection limit was as low as 3 μM. Iron is a very important metal ion cofactor in human body, which is necessary for hemoglobin synthesis. High levels of iron can cause damage to the heart, liver and pancreas, mental decline and protein degeneration [64]. Xin et al. synthesized hydrogels through the hydrogen bond interaction between $(NH_4)_9[Ag_9(MBA)_9]$ and phthalic acid, which can be used as an excellent sensor for Fe^{3+} with a detection limit of 0.611 μM [52]. Interestingly, hollow tubes were formed in Ag_9-NCs/PA hydrogels due to the hydrogen bonds. The absorption peak of Fe^{3+} overlapped with the absorption range of hydrogel, which reduced the energy transfer efficiency. Therefore, the fluorescence of Ag_9-NCs/PA hydrogels was quenched. Zinc pollution is mainly from anthropogenic sources. High levels of the element in wastewaters can have a deleterious effect on wheat growth. Excess zinc can also inactivate the soil, reduce the number of bacteria and reduce the role of microorganisms in the soil [65]. Kuppan et al. described non-luminescent AuNCs stabilized by mercaptopropionic acid for visual and fluorescence detection of Zn^{2+} [66]. The coordination between Zn^{2+} and the ligand limited the intramolecular movement, resulting in the synthesis of luminescent NCs within 1 second at room temperature. In addition, the luminescence enhancement was due to aggregation-induced emission (AIE) caused by Zn^{2+}-mediated self-assembly of NCs (Figure 6). The probe showed good selectivity for Zn^{2+} in water. The right amount of sulfur ions can sterilize and disinfect, but too much can also harm skin health. High concentrations of hydrogen sulfide in the air can also cause oxygen deprivation in the brain [67]. Shuang et al. synthesized CuNCs with assembly-induced emission enhancement (AIEE) properties in the presence of S^{2-} [26], because S^{2-} induced SF@CuNCs to assemble into rod-like nanoparticles that inhibited intramolecular motion. The linear response of S^{2-} concentration ranged from 5.0 μM to 110.0 μM, and the detection limit was as low as 0.286 μM. This assembled nanostructure was successfully used to detect S^{2-} of real water samples. Ag ion usually exists in the form of aqueous solution, which is a natural and non-toxic antibacterial agent. It is not easy for it to develop drug resistance, and generally, it does not damage other normal cells during disinfection and sterilization, so it has high safety characteristics [68]. DPA@AgNCs was prepared with D-penicillamine (DPA) as the stabilizer [27]. When Cu^{2+} was added, the aurophilic interaction between Cu and Ag led to

aggregation-induced emission enhancement, and the luminescence of the NCs changed from red to yellow. The addition of Ag^+ disrupted the loose self-assembly structure of NCs, induced the aggregation of CuNCs and significantly quenched the fluorescence of DPA@Ag/CuNCs. The detection limit was as low as 0.03 μM. In addition, sensors based on DPA@Ag/CuNCs can be used to detect Ag^+ in real water samples, with recoveries ranging from 80.3 to 99.0%.

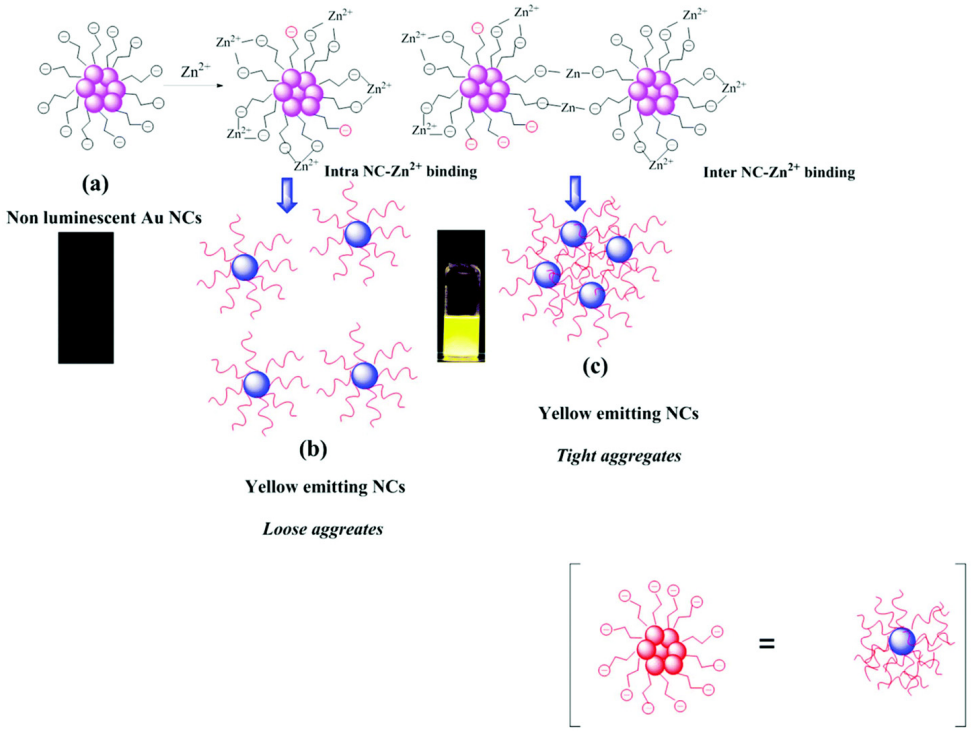


Figure 6. Schematic diagram of self-assembly between AuNCs and Zn^{2+}. (**a**) Non-assembled nonluminescent-NCs, (**b**) Loose aggregates of yellow emitting-NCs, (**c**) Close aggregates of yellow emitting-NCs. Copyright 2017 Royal Society of Chemistry.

3.2. Biomolecules

Biomolecules participate in the constitution of organism and play an important role in biochemical activities. Assembled luminescent NCs were further used to make biomolecular sensors. GSH is present in almost every cell of the body and acts as an important reducing agent to protect proteins in the body. In addition, GSH's nucleophilic properties protect the body from toxins [69]. In 2018, Liu et al. constructed self-assembled Au_5NCs by using poly(amidoamine) that could selectively detect endogenous GSH in cells [59]. The enhanced metallophilic interaction and the rigid structure of the ligand at low temperature were the main reasons for the high fluorescence. As another example, CuNCs prepared by Liu et al. could be self-assembled by the van der Waals forces and dipole interactions in aqueous solution and displayed bright luminescence [56]. GSH could be riveted on the surface of CuNCs and further aggregated the assembled CuNCs through hydrogen bond interaction between the carboxyl and amino groups, resulting in enhanced fluorescence intensity. The detection limit of GSH was as low as 300 nM. In addition, this method can also be used to determine the level of GSH in cells. ALP is widely distributed in human bone, liver, intestine, kidney and other tissues, which is of great significance for the diagnosis of bone and hepatobiliary diseases, especially jaundice diseases [70]. Qu et al. synthesized polyallylamine hydrochloride (PAH)-mediated assembly of GSH-AuNCs to detect ALP activity [21]. The electrostatic interaction between PAH and GSH induced AIE of GSH-AuNCs, and the fluorescence emission of the composite was significantly enhanced. The distance between PAH-AuNCs and 2, 6-dichlorophenol indoxyl (DCIP)

could be narrowed by electrostatic interaction, resulting in fluorescence resonance energy transfer effectively quenching PAH-AuNCs fluorescence. ALP could hydrolyze 2-phospho-L-ascorbic acid (AAP) to L-ascorbic acid (AA), which in turn reduced DCIP from blue to colorless. PAH-AuNCs therefore re-fluoresced, allowing simple and sensitive detection of ALP. This method can be further applied to the analysis of alkaline phosphatase in human serum samples. Protamine is an anticoagulant that can inhibit heparin and stop bleeding but may produce side effects, such as sudden drop in blood pressure, bradycardia and dyspnea. Trypsin can hydrolyze protamine, so sensitive and reliable methods for detecting protamine and trypsin are attracting more and more attention [71]. Xue et al. developed a dual-emission spherical nanohybrid probe (SiNPs@GSH-AuNCs) using electrostatic interactions for the ratio detection of protamine and trypsin [17]. The assembled GSH-AuNCs showed enhanced fluorescence due to AIE, while the blue fluorescence of SiNPs was not affected. The positively charged protamine and Si NPs competed for adsorption to the surface of GSH-AuNCs, inhibiting the self-assembly of SiNPs@GSH-AuNCs and thus leading to fluorescence quenching of GSH-AuNCs. Trypsin restored the AIE of SiNPs@GSH-AuNCs by hydrolyzing protamine. The detection limits of protamine and trypsin were as low as 0.07 μg/mL and 4.50 ng/mL, respectively. Due to the AIEE characteristics and dual-emission fluorescence, the assembly had good sensitivity and selectivity and could successfully detect protamine and trypsin in human serum samples.

Amphiphilic molecules with both hydrophilic and hydrophobic groups can be assembled into ordered aggregates [72,73]. Therefore, introducing amphiphilicity into metallic NCs may enhance the fluorescence of NCs. Xie et al. prepared ultra-bright Au NCs by combining $Au_{22}(SG)_{18}$ with hydrophobic tetraoctyl ammonium (TOA^+) cations [74]. This was the first report of the introduction of amphiphilism into precious metal NCs. Xin et al. prepared Ag_6@C_{16}mim-NCs using 1-hexadecyl-3-methylimidazolium bromide (C_{16}mimBr) modified $[(NH_4)_6[Ag_6(mna)_6]$ [28]. Ag_6@C_{16}mim-NCs luminescence was induced by anion-Π stacking of the surfactant (C_{16}mimBr) around the cluster core. The amphiphilic properties of Ag_6@C_{16}mimNCs enabled it to self-assemble into homogeneous nanosheets and nanorods in a binary solvent of water/dimethyl sulphoxide (DMSO). The assembly showed AIEE due to the limited intramolecular vibration of the ligand, which greatly improved the radiative transition. As shown in Figure 7, arginine could quench the luminescence of Ag_6@C_{16}mim-NCs to a large extent, even in the presence of other amino acids. The dissociation of arginine partially replaced the C_{16}mimBr in water/DMSO, thus leading to the quenching of Ag_6@C_{16}mim-NCs fluorescence. Therefore, Ag_6@C_{16}mimNCs could be used as an effective fluorescent "switch off" probe to detect arginine. Dopamine is the most abundant catecholamine neurotransmitter in the brain, which can regulate various physiological functions of the central nervous system [75]. Two supramolecular complexes with $Ag_{29}LA_{12}$ (LA = a-lipoic acid) and melon bituril (CB) and cyclodextrin (CD) were prepared by Pradeep et al. [57]. $[Ag_{29}(LA)_{12}CB_n]$ formation results from the ability of CB to wrap LA ligands, which depends on dipole–dipole interactions. CD is inserted into the LA cavity to form the $[Ag_{29}(LA)_{12}$@-$CD_n]$ complex, which depends on the van der Waals and hydrogen bond interactions. However, the cavity of CD could wrap the dopamine molecules leading to the quenching of $[Ag_{29}(LA)_{12}$@-$CD_n]$ fluorescence with a detection limit as low as 10 nM.

Histamine has a strong vasodilating effect and plays an important role in regulating allergies and inflammation. When patients are exposed to an allergen, it stimulates the release of histamine, forming edema [76]. Wang et al. developed a Cu3NCs sensor system based on the self-assembly-induced emission (SAIE) for detecting histamine [77]. Because of this strong interaction, electrons are transferred from the Cu nucleus to the ligands and thus quench the luminescence of the CuNCs. More importantly, this method can be used for colorimetric detection of histamine food at levels as low as 5μM. Biothiols play an important role in human physiological activities, and abnormal concentrations have been linked to cancer, Alzheimer's disease, cardiovascular disease and other diseases [78]. In 2021, Wang et al. prepared $Cu_4(TTP)_3$(TPP = 4-(Trifluoromethyl)Thiophenol) and Ni-doped Cu

nanowires (CuNWs) [79]. $Cu_4(TTP)_3$ can self-assemble into nanoribbons (CuNRs) and emit red fluorescence light without Ni addition. The quantum yield of CuNCs was increased nearly fourfold by Ni-Cu metallophilic interaction. In addition, Cys, Hcy and GSH can quench the fluorescence of CuNRs and CuNWs because biothiol can displace ligands from the CuNCs surface by forming strong Cu–S bonds. Therefore, a rapid, sensitive and selective detection of biothiol was realized, and a PL test strip based on CuNCs assembly was developed for colorimetric detection of biothiols. The sensor system and PL test strip were validated in fetal bovine serum samples spiked with biothiols. β-galactosidase (β-Gal) is a glycoside hydrolytic enzyme, which plays an important role in medicine, biotechnology and in the food industry [80]. An aluminum ion coordination-driven AIE of Glutathione-protected CuNCs was reported for the detection of β-Gal [81]. The red-emitting solid CuNCs emitted almost no light in neutral aqueous solutions, but through the self-assembly driven by aluminum cations, CuNCs remained brightly luminous even under neutral conditions, so the assembly could serve as a sensor for the detection of the activity of β-Gal under physiological conditions. β-Gal could hydrolyze p-nitrophenyl b-d-Galactopyranoside (NPGal) to Galactose and p-nitrophenol. The p-nitrophenol is tightly bound to the surface of CuNCs, resulting in fluorescence quenching. Therefore, this assembly can monitor β-Gal levels in real time under physiological conditions.

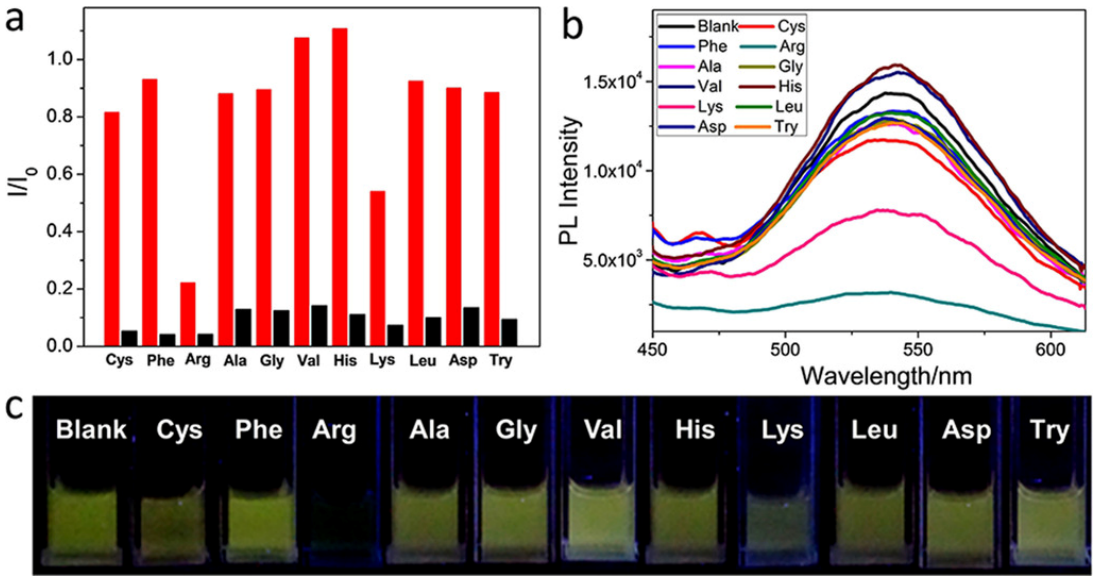


Figure 7. (**a**) The red bars represent the addition of various amino acids to the solution, and the black bars indicate the subsequent addition of Arg to the above solution. (**b**) The luminescence spectra of the Ag_6@C_{16}mimNCs solution after adding different amino acids. (**c**) The photo of the Ag_6@C_{16}mimNCs solution under UV lamp after adding different amino acids. Copyright 2019 Wiley.

3.3. Small Organic Molecule

Chemical, petroleum and coal industries often produce toxic and harmful by-products, which affect the ecosystem in various forms and endanger human health. Therefore, it is very important to develop sensitive and selective sensors to detect these organic compounds. Dithiothreitol is a small-molecule organic reducing agent, which can prevent the formation of protein polymer and inhibit the occurrence of cataract [58]. Xin et al. reported controllable self-assembly of AgNCs into nanowires and vesicles in different solvents [22]. π-π stacking and hydrogen bonding between $[Ag_6(mna)_6]^{6-}$ (Ag_6-NC) and solvents played an important role in the self-assembly. Fe^{3+} could quench the fluorescence of fluorescent vesicles by the internal filtration effect because of the good spectral overlap between Fe^{3+} and Ag_6-NC. Meanwhile, DL-dithiothreitol (DTT) could restore luminescence by reducing Fe^{3+} to Fe^{2+}. Therefore, these fluorescent vesicles could be used as "off/on" sensors to detect Fe^{3+}/DTT. In addition, this study revealed the importance of proton

and aprotic solvents in modulating the morphology of cluster-based assemblies. Organic reagents can act on the human central nervous system, damaging the heart, liver, kidney, and they may cause cancer. Hao et al. induced SAIE of GSH-CuNCs using organic solvents [82]. The assembly made the CuNCs more densely arranged, which limited the vibration and rotation of the cap ligand and enhanced the emission intensity. Different organic reagents induced CuNCs to emit different colors. Nitroimidazoles are a group of nitroimidazole ring-structured drugs that have antibacterial properties, in particular, strong anti-anaerobic activity, as well as antitumor, antiviral and antigenic activities [83]. In 2021, Qi et al. achieved the co-assembly of Ba^{2+} and TBA-AuNCs through coordination, and low-electronegativity Ba^{2+} enhanced the ligand to a metal charge transfer process, so the luminescence intensity of TBA-AuNCs was greatly enhanced [19]. The TBA-AuNCS/Ba^{2+} complex was tested in different imidazole compounds, and only nitroimidazole-containing compounds were found to significantly quench assembly's fluorescence. This was because the nitro group has a strong electron absorption effect and inhibits the ligand-to-metal charge transfer process.

The Ag-chalcogenolate cluster-based (SCC) metal–organic framework can overcome the instability of SCC and extend its sensing applications by using organic molecules as connectors to form SCC-MOFs [84]. In 2018, Zang et al. synthesized a new luminescent Ag sulfide cluster organic skeleton-Ag_{10}bpy, which distincted different fluorescence colors in chloromethane (CH_2Cl_2, $CHCl_3$, and CCl_4) [85]. This was due to the different orientation of the crystal dipole moment of chloromethane relative to chromophore. In another example, Zang et al. reported that a SCC hybrid membrane (Ag_{12}bpz membrane) was prepared by connecting Ag_{12}NCs with a linker containing amino and then using covalent cross-linking between the amino and acrylate monomers [86] (Figure 8). The unstable and almost non-luminous Ag_{12}NCs were transformed into stable yellow luminous Ag_{12}bpz membrane with a significantly higher quantum yield. The increase in the quantum yield can be explained by the rigid environment of the polymer matrix, which effectively inhibits molecular motion and reduces non-radiative relaxation pathways. In addition, with the continuous addition of nitrobenzene, the fluorescence intensity of Ag_{12}bpz film gradually decreased, which was caused by the electron transfer process.

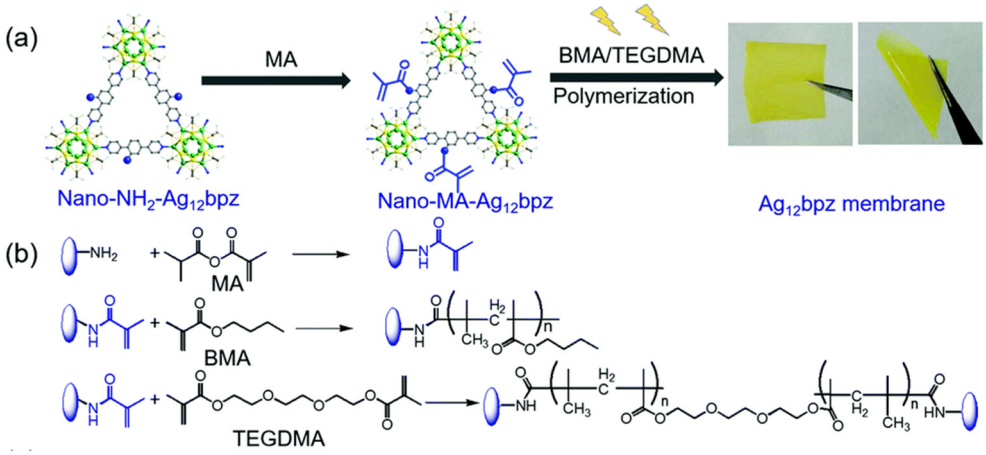


Figure 8. (**a**) The process of preparing Ag_{12}bpz membrane from NH_2-Ag_{12}bpz. (**b**) Post-modification and cross-linking steps. Copyright 2019 Royal Society of Chemistry.

3.4. Gas

Cluster assembly is very important in practical applications, especially for environmental measurements. The realization of common gas sensing is an important goal worth pursuing. Hydrogen sulfide is a flammable and explosive gaseous pollutant. It also plays a variety of physiological functions under normal and pathological conditions [87]. In 2017, Wang et al. synthesized a new nanohybrid using AgNCs and mercapto-modified silica spheres [88]. The surface defects caused by the reaction of sulfide ions with Ag(I)

could quench the blue fluorescence of AgNCs, However, it had no effect on the red fluorescence CdTe QDs encapsulated in silica spheres. This dual-emission fluorescent nanoprobe provides sensitive hydrogen sulfide detection. Due to the different responses of the two components to H_2S, the fluorescence color changed from purple to red. This significant color change made the nanohybrid suitable for rapid detection of H_2S in the field. Hydrogen is of great significance as a clean energy source. However, leakage will cause serious safety problems; therefore, hydrogen detection is of significant interest [89]. Basu et al. reported a Zn^{2+}-induced complex of Au_{14}NCs stabilized by amino acids plus mercaptopropionic acid for hydrogen sensing [23]. The complexation between Zn^{2+} and AuNCs increased the density of the structure and enhanced the luminescence of Au_{14}NCs. Importantly, the fluorescence of Au_{14}NCs was quenched by hydrogen through interaction with Au atoms, and the luminescence recovered after hydrogen desorption. The hydrogen storage capacity of the assembly was 0.244×10^{-3} mM/g at 20 °C and 20 bar. Carbon dioxide is a major component of the atmosphere. However, a large amount of carbon dioxide emitted by human activities causes global warming, which leads to a series of unpredictable global climate changes [90]. Therefore, quantitative detection of carbon dioxide concentration is of great significance. Later, Basu et al. found that Zn^{2+}-induced crystalline materials of Au_{14} could sense and store CO_2 because CO_2 could induce intermittently reversible photoluminescence changes of the assembled clusters, and the adsorption capacity was 1.79 mM/g at 20 bar and 20 °C [91].

SCC-MOF can overcome the instability of Ag NCs and endow MOF with larger channels, which has been applied in sensing. The porous (Ag_{12}bpy)-MOF (bpy = 4, 4′-bipyridine) assembled by Zang et al. could be used as a dual-function luminescence switch. O_2 turned off fluorescence by interacting with the highly permeable channel (Ag_{12}bpy)-MOF [92]. Different volatile organic compounds (VOCs) had different dipole interactions with (Ag_{12}bpy)-MOF, which could turn on fluorescence of different colors. Later, they prepared (Ag_{12}bpy-NH_2)-MOF using 3-amino-4, 4′-bipyridine (bpy-NH_2) ligand engineering on the same NC, and the introduction of the amino group enabled fluorescent-phosphorescent dual emission [93]. The high sensitivity of (Ag_{12}bpy-NH_2)-MOF to oxygen could be used for ratio sensing of oxygen during hypoxia, achieving ultra-fast response to trace oxygen in 0.3 s, with detection limit as low as 0.1 PPM. The further introduction of the -CH_3 group on could extend the sensing range of O_2. Ag_{12}bpy-NH_2/CH_3 functioned in the O_2 concentration range of 20 ppm to 0.1%. This was because the -CH_3 group in (Ag_{12}bpy-CH_3)-MOF interfered with the collision process of oxygen, so oxygen could not effectively quench the fluorescence of (Ag_{12}bpy-CH_3)-MOF (Figure 9).

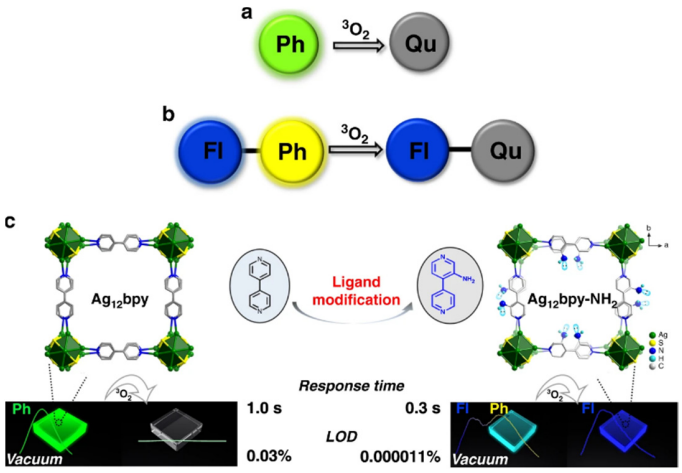


Figure 9. Schematic of $^3O_2$ sensing based on (**a**) a single Ph emission and (**b**) dual Fl-Ph emissions Fl = Fluorescence, Ph = Phosphorescence, Qu = Quenched. (**c**) Schematic of Ag_{12}bpy-NH_2 crystals emitting a single green color under vacuum that is quenched by oxygen with a response time of approximately 1.0 s and an LOD of 0.03%. Copyright 2020 Springer Nature.

3.5. Temperature Sensing

Supramolecular assembly is an effective method to construct multifunctional nanomaterials for sensing temperature. For example, Xin et al. used Ag_9NCs to interact with succinic acid (SA) to construct hydrogels due to argentophilic interactions and non-covalent forces between the peripheral ligands and SA [16]. This caused the highly ordered nanofibers to produce an AIE phenomenon, emitting bright red fluorescence. As the temperature increased, the probability of collision between the solvent molecules or oxygen molecules and the luminescence center increased, and the weakening of the non-covalent force led to the destruction of gel network, which led to the weakening of fluorescence of Ag_9NCs. At present, metal NCs as a fluorescent probe for temperature mainly stayed at ultra-low temperature for temperature detection, while the luminescent hydrogel prepared in this paper had good sensitivity to high temperature (20–100 °C) (Figure 10). Later, Xin et al. induced $Ag_9(mba)_9$ (H_2mba = 2-mercaptobenzoic acid) self-assembly by peptide DD-5 for temperature sensing [20]. The non-luminescent Ag_9NCs and DD-5 constructed the luminescent hydrogel through the non-covalent force and argentophilic interaction. With the increase in temperature, in addition to the increase in collision probability between oxygen molecules and luminescence center, the weakening of the non-covalent force led to the destruction of gel network. High temperature also led to the reduction in charge transfer from the ligand to the Ag nucleus and the oxidation of Ag_9-NCs into AgNPs. These reasons led to the weakening of fluorescence of Ag_9NC. The dry gel showed a good linear relationship at low temperature (−160−80 °C) and high temperature (80−260 °C), respectively. Therefore, Ag_9NCS/DD-5 dry gel showed good performance at both low and high temperatures.

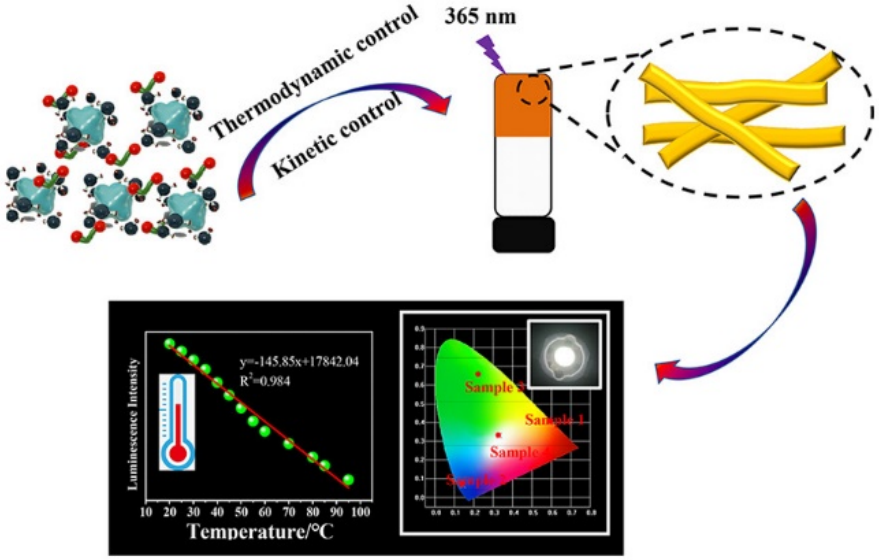


Figure 10. Ag_9NCs/SA hydrogel can be used as a temperature-controlled detector and as a light-emitting diode conversion material together with phosphor. Copyright 2020 American Chemical Society.

As new luminescent nanomaterials, the AuNCs assembly can also be used to sense temperature. The synthesis of highly luminescent AuNCs is of great significance. Shang et al. reported that AuNCs assembled using peptides as templates significantly improved luminescence efficiency [94]. The AuNCs were assembled into a fibrous state because of the hydrophobic interaction between the peptides and ethanol. The luminescence intensity of the self-assembled AuNCs increased nearly 70 times, and the luminescence intensity and quantum lifetime changed with the increase in temperature. In addition, Xin et al. prepared a fluorescent hybrid nanomaterial (CD/AuNC) through the electrostatic interaction between carbon dots (CDs) and GSH-AuNCs [53]. Under the excitation of

380 nm, CD/AuNC exhibited red and blue emission behaviors (455 nm and 600 nm). Dual-emission fluorescent probes prepared by chemical cross-linking require complex modification and synthesis [95]. The dual-emission detector prepared in this paper solves these problems perfectly. As the temperature increased, the molecular collision frequency and non-radiative transition rate increased, the radiative transition rate remained constant, the emission intensity of AuNCs was reduced, while CDs emission was not affected. The temperature colorimetry in the range of 20 °C ~ 80 °C showed high reproducibility. CD/AuNC had good biocompatibility and high stability, which could be further used in intracellular temperature detection.

3.6. pH

In addition, the NC assembly can also be used for sensing pH. Qi et al. used chiral cysteine-modified AuNCs to self-assemble into ordered microflowers due to the coordination and electrostatic interactions between Cd^{2+}/H^{+} and the ligands [54]. Interestingly, the circular dichroismand photoluminescence signals of microflowers could both respond to pH. This dual-mode sensitive platform could not only sense pH, but it could also be used for information encryption and decryption. In another example, Jiang et al. quickly synthesized triangular supramolecular MMI-CuNCs (MMI = 2-mercapto-1-methylimidazole) using ionic liquid (ILs)-[Bmim]BF_4 in 30 seconds [55]. This was due to the electrostatic interaction between positive [Bmim]BF_4 and negative MMI-CuNCs, and the high polarizability and hydrophobicity of [Bmim]BF_4 could increase the nucleation rate and reaction rate of MMI-CuNCs precursor. Interestingly, the prepared assembly was sensitive to pH and produced different photoluminescence intensity in the pH range of 4–12. So, MMI-CuNCs/[Bmim]BF_4 could be used to measure changes in pH.

A summary of the performances of the assembled NCs-based sensors is shown in Table 2.

Table 2. Comparison of the analytical performances of assembled NCs sensors.

NCs	Fluorescent	Detection Analyte	Detection Limit	Detection Range	The Practical Application
TSA-AgNCs [18]	Red	Hg^{2+}	91.3 nM	0.3–2.2 μM	No
SA-AgNCs [61]	Orange	Hg^{2+}	3.1 nM	3.5–100 nM	Tap water, Lactating mother's milk
CuNCs [51]	Red	Hg^{2+}	0.3 nM	1–500 nM	Tap water, Lake water, wastewater
Ag_6NCs [63]	Blue	Al^{3+}	3.13 μM	No	No
$(NH_4)_9[Ag_9(MBA)_9]$ [52]	Red	Fe^{3+}	0.611 μM	0–6 μM	No
AuNCs [66]	Yellow/green	Zn^{2+}	9 nM	0.2–1 μM	No
SF@CuNCs [26]	Blue	S^{2-}	0.286 μM	5.0–110.0 μM	Tap water, River waste
DPA@Ag NCs [27]	Red to yellow	Ag^{+}	0.03 μM	0.05–800 μM	Tap water, Post-sewage water, Lake water
Poly-Au_5 [59]	Red	GSH	0.56 μM	0–10 μM	HeLa cells
CuNCs [56]	Red	GSH	300 nM	1–100 μM	Three kinds of human cell lines
GSH-AuNCs [21]	Yellow	ALP	0.2 U/L	0.5–80 U/L	Human serum
GSH-AuNCs [17]	Yellow	Protamine and trypsin	0.07 μg/mL 4.50 ng/mL	0.15–3 μg/mL, 10–100 ng/mL	Human serum
$(NH_4)_6[Ag_6(mna)_6]$ [28]	Yellow	Arginine	28 μM	0–200 μM	No
$Ag_{29}LA_{12}$ [57]	Red	Dopamine	10 nM	0–100 nM	No
Cu_3NCs [77]	Yellow	Histamine	60 nM	0.1–10 μM	Fish, Shrimp, Red wine

Table 2. *Cont.*

NCs	Fluorescent	Detection Analyte	Detection Limit	Detection Range	The Practical Application
$Cu_4(TTP)_3$ [79]	Red	Biothiols	0.01 μM 0.01 μM 0.1 μM	0.1–100 μM 1–100 μM 1–1000 μM	Fetal bovine serum
GSH-CuNCs [81]	Red	β-galactosidase	0.7 U L^{-1}	2.3 U L^{-1}–96.0 U L^{-1}	No
$[Ag_6(mna)_6]^{6-}$ [22]	Blue	Dithiothreit-ol	0.11 mM	No	No
TBA-AuNCs [19]	Yellow	2-methyl-4-nitroimidazole	13.8 μM	0–400 μM	No
GSH-AgNCs [88]	Blue	H_2S	32 nM	0–3 μM	No
$[Ag_9(mba)_9]$ [16]	Orange-red	Temperature	No	20–100 °C	No
$[Ag_9(mba)_9]$ [20]	Orange-red	Temperature	No	−160–(−80 °C) 80–260 °C	No
Peptide-AuNCs [94]	Red	Temperature	No	10–45 °C	HeLa cells
GSH-AuNCs [53]	Red	Temperature	No	20–80 °C	Living cells
Cys-AuNCs [54]	Red	pH	No	6.7–10.5	No
CuNCs@MMI [55]	Blue	pH	No	4–12	No

4. Conclusions and Future Perspectives

Coinage metal NCs play an important role in nanomaterials science due to their structural regularity and unique chemical properties. With the development of new methods for synthesis, surface functionalization and purification of precious metal NCs, NCs have been used in catalysis, therapy, diagnosis, sensing, light-emitting devices and molecular recognition. In addition, the well-defined structure, excellent photoelectric properties and ready availability of a variety of ligands make metal NCs excellent building blocks. Assembly is an effective strategy for directing NCs into specific structures. It is of great significance to realize the ordered assembly of NCs following various chemical principles. NC assembly technology was reviewed in detail to build different types of sensors. A series of supramolecular interactions provide the driving forces for the self-assembly of NCs, such as hydrogen bonding, electrostatic attraction, van der Waals force, C–H···π/π···π and metallophilic interactions. The assembled superstructures exhibit useful physicochemical properties, such as aggregation-induced emission, enhanced circularly polarized luminescence and optical absorption, enhanced stability and mechanical strength. These properties were effectively applied to sensing metal ions, biomolecules, organic molecules, gas, temperature and pH.

Despite recent achievements, the development of cluster assemblies faces several challenges, not least in the synthesis, separation and purification of monodispersed clusters. The relationships between the atomic structure and the corresponding chemical properties of the clusters are yet to be elucidated. Electrostatic attraction-based assembly usually leads to irreversible aggregation of metal NCs. Understanding the assembly details of water-soluble NCs at the molecular level is more difficult because of the absence of crystal structures. The assembly of metal NCs is susceptible to the surroundings and can be easily assembled into by-products, such as large nanoparticles and irregular structures, due to the large surface energy of metal NCs and weak interactions between their ligand shells. Most NC assemblies are large in size, limiting their in vivo biomedical applications. Therefore, the synthesis and assembly of precious metal NCs need to be further optimized to control their morphology and complex properties. For example, the production of highly ordered assembled metal NCs and the development of polydentate ligands could result in the strengthening of the interaction between ligand shells with resulting stable regular structures of the metal NCs.

The development and deployment of metal NCs-based optical sensors could contribute to better medical diagnosis, sensitive environmental monitoring and provide useful information that could lead to an in-depth understanding of a variety of industrial processes.

Author Contributions: Conceptualization, C.R. and T.S.; validation, T.S. and L.S.; formal analysis, X.D. and L.Y.; writing—original draft preparation, C.R., T.S.; writing—review and editing, T.S. and L.S.; supervision, T.S.; project administration, T.S. and X.Z.; funding acquisition, T.S. and X.Z. All authors have read and agreed to the published version of the manuscript.

Funding: This research received no external funding.

Institutional Review Board Statement: Not applicable.

Informed Consent Statement: Not applicable.

Data Availability Statement: Not applicable.

Acknowledgments: We acknowledge funding from the National Natural Science Foundation of China (21904011, 21890742, 82061138005 and 21727815), the Shenzhen Science and Technology Innovation Commission (20200809233237001, 20200822212355001 and 20200812180434001) and Shenzhen Key Laboratory for Nano-Biosensing Technology (ZDSYS20210112161400001).

Conflicts of Interest: The authors declare no conflict of interest.

References

1. Li, D.; Chen, Z.; Mei, X. Fluorescence enhancement for noble metal nanoclusters. *Adv. Colloid Interface Sci.* **2017**, *250*, 25–39. [CrossRef] [PubMed]
2. Yao, Q.; Wu, Z.; Liu, Z.; Lin, Y.; Yuan, X.; Xie, J. Molecular reactivity of thiolate-protected noble metal nanoclusters: Synthesis, self-assembly, and applications. *Chem. Sci.* **2021**, *12*, 99–127. [CrossRef] [PubMed]
3. Liu, H.; Hong, G.; Luo, Z.; Chen, J.; Chang, J.; Gong, M.; He, H.; Yang, J.; Yuan, X.; Li, L.; et al. Atomic-Precision Gold Clusters for NIR-II Imaging. *Adv. Mater.* **2019**, *31*, 1901015. [CrossRef]
4. Li, J.; Zhang, S.; Yu, Y.; Wang, Y.; Zhang, L.; Lin, B.; Guo, M.; Cao, Y. A novel universal nanoplatform for ratiometric fluorescence biosensing based on silver nanoclusters beacon. *Chem. Eng. J.* **2020**, *391*, 123526. [CrossRef]
5. Zhao, L.; Ma, Z. New immunoprobes based on bovine serum albumin-stabilized copper nanoclusters with triple signal amplification for ultrasensitive electrochemical immunosensing for tumor marker. *Sens. Actuators B Chem.* **2017**, *241*, 849–854. [CrossRef]
6. Higaki, T.; Li, Y.; Zhao, S.; Li, Q.; Li, S.; Du, X.; Yang, S.; Chai, J.; Jin, R. Atomically Tailored Gold Nanoclusters for Catalytic Application. *Angew. Chem. Int. Ed.* **2019**, *58*, 8291–8302. [CrossRef]
7. Khrizanforov, M.N.; Fedorenko, S.V.; Mustafina, A.R.; Kholina, K.V.; Nizamee, I.R.; Strekalova, S.O.; Grinenko, V.V.; Gryaznova, T.V.; Zairov, R.R.; Mazzaro, R.; et al. Silica-Supported Silver Nanoparticles as an Efficient Catalyst for Aromatic C-H Alkylation and Fluoroalkylation. *Dalton Trans.* **2018**, *47*, 9608.
8. Xie, J.; Zheng, Y.; Ying, J. Protein-Directed Synthesis of Highly Fluorescent Gold Nanoclusters. *J. Am. Chem. Soc.* **2009**, *131*, 888–889. [CrossRef]
9. Meng, L.; Zhu, Q.; Yin, J.; Xu, N. Polyethyleneimine protected silver nanoclusters luminescence probe for sensitive detection of cobalt (II) in living cells. *J. Photochem. Photobiol. B Biol.* **2017**, *173*, 508–513.
10. Basu, K.; Paul, S.; Jana, R.; Datta, A.; Banerjee, A. Red-Emitting Copper Nanoclusters: From Bulk-Scale Synthesis to Catalytic Reduction. *ACS Sustain. Chem. Eng.* **2018**, *7*, 1998–2007. [CrossRef]
11. Halawa, M.I.; Lai, J.; Xu, G. Gold nanoclusters: Synthetic strategies and recent advances in fluorescent sensing. *Mater. Today Nano* **2018**, *3*, 9–27. [CrossRef]
12. Chatterjee, S.; Lou, X.; Liang, F.; Yang, Y. Surface-functionalized gold and silver nanoparticles for colorimetric and fluorescent sensing of metal ions and biomolecules. *Coord. Chem. Rev.* **2022**, *459*, 214461. [CrossRef]
13. Chen, P.; Periasamy, A.P.; Harroun, S.G.; Wu, W.; Chang, H. Photoluminescence sensing systems based on copper, gold and silver nanomaterials. *Coord. Chem. Rev.* **2016**, *320–321*, 129–138. [CrossRef]
14. Rehman, A.; Zeng, X. Interfacial composition, structure, and properties of ionic liquids and conductive polymers for the construction of chemical sensors and biosensors: A perspective. *Curr. Opin. Electrochem.* **2020**, *23*, 47–56. [CrossRef]
15. Li, J.; He, J.; Zhang, C.; Chen, J.; Mao, W.; Yu, C. Dual-type responsive electrochemical biosensor for the detection of alpha2,6-sialylated glycans based on AuNRs-SA coupled with c-SWCNHs/S-PtNC nanocomposites signal amplification. *Biosens. Bioelectron.* **2019**, *130*, 166–173. [CrossRef] [PubMed]
16. Sun, P.; Wang, Z.; Bi, Y.; Sun, D.; Zhao, T.; Zhao, F.; Wang, W.; Xin, X. Self-Assembly-Driven Aggregation-Induced Emission of Silver Nanoclusters for Light Conversion and Temperature Sensing. *ACS Appl. Nano Mater.* **2020**, *3*, 2038–2046. [CrossRef]

17. Xue, F.; Qu, F.; Han, W.; Xia, L.; You, J. Aggregation-induced emission enhancement of gold nanoclusters triggered by silicon nanoparticles for ratiometric detection of protamine and trypsin. *Anal. Chim. Acta* **2019**, *1046*, 170–178. [CrossRef]
18. Pan, S.; Liu, W.; Tang, J.; Yang, Y.; Feng, H.; Qian, Z.; Zhou, J. Hydrophobicity-guided self-assembled particles of silver nanoclusters with aggregation-induced emission and their use in sensing and bioimaging. *J. Mater. Chem. B* **2018**, *6*, 3927–3933. [CrossRef]
19. Shen, J.; Bi, Y.; Zhang, H.; Xu, L.; Feng, J.; Qi, W. A sensitive chemosensor for nitro-containing compounds based on Au nanoclusters/Ba^{2+} co-assembly system: The crucial role of ligands to metal charge transfer. *Colloids Surf. A Physicochem. Eng Asp.* **2021**, *627*, 127160. [CrossRef]
20. Wang, W.; Wang, Z.; Sun, D.; Li, S.; Deng, Q.; Xin, X. Supramolecular Self-Assembly of Atomically Precise Silver Nanoclusters with Chiral Peptide for Temperature Sensing and Detection of Arginine. *Nanomaterials* **2022**, *12*, 424. [CrossRef]
21. Han, X.; Han, M.; Ma, L.; Qu, F.; Kong, R.; Qu, F. Self-assembled gold nanoclusters for fluorescence turn-on and colorimetric dual-readout detection of alkaline phosphatase activity via DCIP-mediated fluorescence resonance energy transfer. *Talanta* **2019**, *194*, 55–62. [CrossRef]
22. Shen, J.; Wang, Z.; Sun, D.; Liu, G.; Yuan, S.; Kurmoo, M.; Xin, X. Self-assembly of water-soluble silver nanoclusters: Superstructure formation and morphological evolution. *Nanoscale* **2017**, *9*, 19191–19200. [CrossRef] [PubMed]
23. Basu, S.; Paul, A.; Chattopadhyay, A. Zinc mediated crystalline assembly of gold nanoclusters for expedient hydrogen storage and sensing. *J. Mater. Chem. A* **2016**, *4*, 1218–1223. [CrossRef]
24. Ariga, K.; Nishikawa, M.; Mori, T.; Takeya, J.; Shrestha, L.K.; Hill, J.P. Self-assembly as a key player for materials nanoarchitectonics. *Sci. Technol. Adv. Mater.* **2019**, *20*, 51–95. [CrossRef] [PubMed]
25. Wang, T.; Zhuang, J.; Lynch, J.; Chen, O.; Wang, Z.; Wang, X.; LaMontagne, D.; Wu, H.; Wang, Z.; Cao, Y.C. Self-Assembled Colloidal Superparticles from Nanorods. *Scinece* **2012**, *338*, 358–363. [CrossRef] [PubMed]
26. Zhang, G.; Wang, R.; Shi, L.; Zhang, C.; Zhang, Y.; Zhou, Y.; Dong, C.; Li, G.; Shuang, S. Aggregation/assembly induced emission based on silk fibroin-templated fluorescent copper nanoclusters for "turn-on" detection of S^{2-}. *Sens. Actuators B Chem.* **2019**, *279*, 361–368. [CrossRef]
27. An, M.; Li, H.; Su, M.; Gao, S.; Wang, M.; Shen, S.; Gao, Z.; Dong, J. Cu^{2+} enhanced fluorescent Ag nanoclusters with tunable emission from red to yellow and the application for Ag^{+} sensing. *Spectrochim. Acta A Mol. Biomol. Spectrosc.* **2021**, *252*, 119484. [CrossRef]
28. Shen, J.; Wang, Z.; Xia, C.; Sun, D.; Yuan, S.; Xin, X. Amphiphilicity Regulation of Ag(I) Nanoclusters: Self-Assembly and Its Application as a Luminescent Probe. *Chem. Eur. J.* **2019**, *25*, 4713–4721. [CrossRef]
29. Ghosh, D.; Ganayee, M.A.; Som, A.; Srikrishnarka, P.; Murali, N.; Bose, S.; Chakraborty, A.; Mondal, B.; Ghosh, P.; Pradeep, T. Hierarchical Assembly of Atomically Precise Metal Clusters as a Luminescent Strain Sensor. *ACS Appl. Mater. Interfaces* **2021**, *13*, 6496–6504. [CrossRef]
30. Liu, J.; Tian, Y.; Ai, L.; Wu, Z.; Yao, D.; Liu, Y.; Yang, B.; Zhang, H. Self-Assembly of Au Nanoclusters into Helical Ribbons by Manipulating the Flexibility of Capping Ligands. *Langmuir* **2020**, *36*, 14614–14622. [CrossRef]
31. Chen, T.; Yang, S.; Li, Q.; Song, Y.; Li, G.; Chai, J.; Zhu, M. A double helical 4H assembly pattern with secondary hierarchical complexity in an Ag70 nanocluster crystal. *Nanoscale Horiz.* **2021**, *6*, 913–917. [CrossRef] [PubMed]
32. Wu, Z.; Li, Y.; Liu, J.; Lu, Z.; Zhang, H.; Yang, B. Colloidal self-assembly of catalytic copper nanoclusters into ultrathin ribbons. *Angew. Chem. Int. Ed.* **2014**, *53*, 12196–12200. [CrossRef] [PubMed]
33. Xie, Z.; Sun, P.; Wang, Z.; Li, H.; Yu, L.; Sun, D.; Chen, M.; Bi, Y.; Xin, X.; Hao, J. Metal-Organic Gels from Silver Nanoclusters with Aggregation-Induced Emission and Fluorescence-to-Phosphorescence Switching. *Angew. Chem. Int. Ed.* **2020**, *59*, 9922–9927. [CrossRef] [PubMed]
34. Zhang, C.; Zhang, A.; Hou, W.; Li, T.; Wang, K.; Zhang, Q.; Fuente, J.M.; Jin, W.; Cui, D. Mimicking Pathogenic Invasion with the Complexes of $Au_{22}(SG)_{18}$-Engineered Assemblies and Folic Acid. *ACS Nano* **2018**, *12*, 4408–4418. [CrossRef] [PubMed]
35. Wei, X.; Kang, X.; Yuan, Q.; Qin, C.; Jin, S.; Wang, S.; Zhu, M. Capture of Cesium Ions with Nanoclusters: Effects on Inter- and Intramolecular Assembly. *Chem. Mater.* **2019**, *31*, 4945–4952. [CrossRef]
36. Xu, M.; Jia, T.; Li, B.; Ma, W.; Chen, X.; Zhao, X.; Zang, S. Tuning the properties of atomically precise gold nanoclusters for biolabeling and drug delivery. *ChemComm* **2020**, *56*, 8766–8769. [CrossRef]
37. Yuan, J.; Liu, Z.; Dong, M.; Wang, L.; Dong, S.; Hao, J. Self-Assembly of Amphiphilic Copper Nanoclusters Driven by Cationic Surfactants. *Langmuir* **2021**, *37*, 6613–6622. [CrossRef]
38. AbdulHalim, L.G.; Bootharaju, M.S.; Tang, Q.; Del Gobbo, S.; AbdulHalim, R.G.; Eddaoudi, M.; Jiang, D.E.; Bakr, O.M. $Ag_{29}(BDT)_{12}(TPP)_4$: A Tetravalent Nanocluster. *J. Am. Chem. Soc.* **2015**, *137*, 11970–11975. [CrossRef]
39. Li, Q.; Russell, J.C.; Luo, T.; Roy, X.; Rosi, N.L.; Zhu, Y.; Jin, R. Modulating the hierarchical fibrous assembly of Au nanoparticles with atomic precision. *Nat. Commun.* **2018**, *9*, 3871. [CrossRef]
40. Huang, J.; Wang, Z.; Zang, S.; Mak, T.C.W. Spontaneous Resolution of Chiral Multi-Thiolate-Protected Ag_{30}Nanoclusters. *ACS Cent. Sci.* **2020**, *6*, 1971–1976. [CrossRef]
41. Wu, Z.; Du, Y.; Liu, J.; Yao, Q.; Chen, T.; Cao, Y.; Zhang, H.; Xie, J. Aurophilic Interactions in the Self-Assembly of Gold Nanoclusters into Nanoribbons with Enhanced Luminescence. *Angew. Chem. Int. Ed.* **2019**, *58*, 8139–8144. [CrossRef] [PubMed]

42. Das, A.K.; Maity, S.; Sengupta, T.; Bista, D.; Reber, A.C.; Patra, A.; Khanna, S.N.; Mandal, S. One-Dimensional Silver-Thiolate Cluster-Assembly: Effect of Argentophilic Interactions on Excited-State Dynamics. *J. Phys. Chem. Lett.* **2021**, *12*, 2154–2159. [CrossRef] [PubMed]
43. Wu, Z.; Liu, J.; Gao, Y.; Liu, H.; Li, T.; Zou, H.; Wang, Z.; Zhang, K.; Wang, Y.; Zhang, H.; et al. Assembly-Induced Enhancement of Cu Nanoclusters Luminescence with Mechanochromic Property. *J. Am. Chem. Soc.* **2015**, *137*, 12906–12913. [CrossRef] [PubMed]
44. Zhou, T.; Zhu, J.; Gong, L.; Nong, L.; Liu, J. Amphiphilic Block Copolymer-Guided in Situ Fabrication of Stable and Highly Controlled Luminescent Copper Nanoassemblies. *J. Am. Chem. Soc.* **2019**, *141*, 2852–2856. [CrossRef]
45. Jin, R.; Zeng, C.; Zhou, M.; Chen, Y. Atomically Precise Colloidal Metal Nanoclusters and Nanoparticles: Fundamentals and Opportunities. *Chem. Rev.* **2016**, *116*, 10346–10413. [CrossRef]
46. Whitesides, G.M.; Grzybowski, B. Self-Assembly at All Scales. *Science* **2002**, *295*, 2418–2421. [CrossRef]
47. Winterton, R.H.S. Van der Waals forces. *Contemp. Phys.* **1970**, *11*, 559–574. [CrossRef]
48. Li, Y.; Zhou, M.; Song, Y.; Higaki, T.; Wang, H.; Jin, R. Double-helical assembly of heterodimeric nanoclusters into supercrystals. *Nature* **2021**, *594*, 380–384. [CrossRef]
49. Tsuzuki, S. CH/π interactions. *Annu. Rep. Sect. "C" (Phys. Chem.)* **2012**, *108*, 69–95. [CrossRef]
50. Sculfort, S.; Braunstein, P. Intramolecular d^{10}-d^{10} interactions in heterometallic clusters of the transition metals. *Chem. Soc. Rev.* **2011**, *40*, 2741–2760. [CrossRef]
51. Wang, H.; Bai, H.; Wang, Y.; Gan, T.; Liu, Y. Highly selective fluorimetric and colorimetric sensing of mercury(II) by exploiting the self-assembly-induced emission of 4-chlorothiophenol capped copper nanoclusters. *Mikrochim. Acta* **2020**, *187*, 185. [CrossRef] [PubMed]
52. Cheng, X.; Sun, P.; Zhang, N.; Zhou, S.; Xin, X. Self-assembly of silver nanoclusters and phthalic acid into hollow tubes as a superior sensor for Fe^{3+}. *J. Mol. Liq.* **2021**, *323*, 115032. [CrossRef]
53. Jia, Y.; Zhang, X.; Yin, C.; Zhang, X.; Zhang, J.; Wang, X.; Xin, J. An electrostatic self-assembly route to prepare C-dots/gold nanoclusters for dual-emission ratiometric optical thermometry in living cells. *Anal. Methods* **2019**, *11*, 3974–3980. [CrossRef]
54. Shen, J.; Xiao, Q.; Sun, P.; Feng, J.; Xin, X.; Yu, Y.; Qi, W. Self-Assembled Chiral Phosphorescent Microflowers from Au Nanoclusters with Dual-Mode pH Sensing and Information Encryption. *ACS Nano* **2021**, *15*, 4947–4955. [CrossRef]
55. Han, B.; Yan, Q.; Xin, Z.; Yan, Q.; Jiang, J. Ionic Liquids-Assisted Highly Luminescent Copper Nanoclusters with Triangle Supramolecular Nanostructures. *Chin. J. Chem.* **2021**, *39*, 1867–1870. [CrossRef]
56. Wang, H.; Mao, A.; Gan, T.; Liu, Y. A turn-on fluorescence strategy for cellular glutathione determination based on the aggregation-induced emission enhancement of self-assembled copper nanoclusters. *Analyst* **2020**, *145*, 7009–7017. [CrossRef]
57. Nag, A.; Chakraborty, P.; Thacharon, A.; Paramasivam, G.; Mondal, B.; Bodiuzzaman, M.; Pradeep, T. Atomically Precise Noble Metal Cluster-Assembled Superstructures in Water: Luminescence Enhancement and Sensing. *J. Phys. Chem. C* **2020**, *124*, 22298–22303. [CrossRef]
58. Araujo, J.E.; Lopez-Fernandez, H.; Diniz, M.S.; Baltazar, P.M.; Pinheiro, L.C.; da Silva, F.C.; Carrascal, M.; Videira, P.; Santos, H.M.; Capelo, J.L. Dithiothreitol-based protein equalization technology to unravel biomarkers for bladder cancer. *Talanta* **2018**, *180*, 36–46. [CrossRef]
59. Yang, L.; Wang, H.; Li, D.; Li, L.; Lou, X.; Liu, H. Self-Nucleation and Self-Assembly of Highly Fluorescent Au_5 Nanoclusters for Bioimaging. *Chem. Mater.* **2018**, *30*, 5507–5515. [CrossRef]
60. Zhang, Y.; Jiang, H.; Wang, X. Cytidine-stabilized gold nanocluster as a fluorescence turn-on and turn-off probe for dual functional detection of Ag^+ and Hg^{2+}. *Anal. Chim. Acta* **2015**, *870*, 1–7. [CrossRef]
61. Packirisamy, V.; Pandurangan, P. Heterocyclic thiol protected supramolecular self-assembly of silver nanoclusters for ultrasensitive detection of toxic Hg (II) ions in nanomolar range. *J. Mol. Liq.* **2021**, *344*, 117769. [CrossRef]
62. Sieg, H.; Ellermann, A.L.; Maria Kunz, B.; Jalili, P.; Burel, A.; Hogeveen, K.; Bohmert, L.; Chevance, S.; Braeuning, A.; Gauffre, F.; et al. Aluminum in liver cells—The element species matters. *Nanotoxicology* **2019**, *13*, 909–922. [CrossRef]
63. Shen, J.; Wang, Z.; Sun, D.; Xia, C.; Yuan, S.; Sun, P.; Xin, X. pH-Responsive Nanovesicles with Enhanced Emission Co-Assembled by Ag(I) Nanoclusters and Polyethyleneimine as a Superior Sensor for Al^{3+}. *ACS Appl. Mater. Interfaces* **2018**, *10*, 3955–3963. [CrossRef] [PubMed]
64. Grant, E.S.; Clucas, D.B.; McColl, G.; Hall, L.T.; Simpson, D.A. Re-examining ferritin-bound iron: Current and developing clinical tools. *Clin. Chem. Lab. Med.* **2021**, *59*, 459–471. [CrossRef]
65. Hu, W.; Niu, Y.; Zhu, H.; Dong, K.; Wang, D.; Liu, F. Remediation of zinc-contaminated soils by using the two-step washing with citric acid and water-soluble chitosan. *Chemosphere* **2021**, *282*, 131092. [CrossRef] [PubMed]
66. Kuppan, B.; Maitra, U. Instant room temperature synthesis of self-assembled emission-tunable gold nanoclusters: Million-fold emission enhancement and fluorimetric detection of Zn^{2+}. *Nanoscale* **2017**, *9*, 15494–15504. [CrossRef] [PubMed]
67. Xiao, Q.; Wang, T.; Yu, S.; Yi, P.; Li, L. Influence of UV lamp, sulfur(IV) concentration, and pH on bromate degradation in UV/sulfite systems: Mechanisms and applications. *Water Res.* **2017**, *111*, 288–296. [CrossRef]
68. Cui, J.; Shao, Y.; Zhang, H.; Zhang, H.; Zhu, J. Development of a novel silver ions-nanosilver complementary composite as antimicrobial additive for powder coating. *Chem. Eng. J.* **2021**, *420*, 127633. [CrossRef]
69. Berndt, C.; Lillig, C.H. Glutathione, Glutaredoxins, and Iron. *Antioxid. Redox Signal.* **2017**, *27*, 1235–1251. [CrossRef]
70. Siller, A.F.; Whyte, M.P. Alkaline Phosphatase: Discovery and Naming of Our Favorite Enzyme. *J. Bone Miner. Res.* **2018**, *33*, 362–364. [CrossRef]

71. Zhou, J.; Zhang, F.; Zhao, R.; Liu, S.; Li, W.; He, F.; Gai, S.; Yang, P. A novel "off-on-off" fluorescent sensor based on inner filter effect for ultrasensitive detection of protamine/trypsin and subcellular colocalization. *Sens. Actuators B Chem.* **2021**, *340*, 129930. [CrossRef]
72. Du, J.; O'Reilly, R.K. Advances and challenges in smart and functional polymer vesicles. *Soft Matter* **2009**, *5*, 3544–3561. [CrossRef]
73. Liao, H.; Lin, J.; Liu, Y.; Huang, P.; Jin, A.; Chen, X. Self-assembly mechanisms of nanofibers from peptide amphiphiles in solution and on substrate surfaces. *Nanoscale* **2016**, *8*, 14814–14820. [CrossRef] [PubMed]
74. Yao, Q.; Yuan, X.; Yu, Y.; Yu, Y.; Xie, J.; Lee, J. Introducing amphiphilicity to noble metal nanoclusters via phase-transfer driven ion-pairing reaction. *J. Am. Chem. Soc.* **2015**, *137*, 2128–2136. [CrossRef]
75. Gershman, S.J.; Uchida, N. Believing in dopamine. *Nat. Rev. Neurosci.* **2019**, *20*, 703–714. [CrossRef]
76. Obara, I.; Telezhkin, V.; Alrashdi, I.; Chazot, P.L. Histamine, histamine receptors, and neuropathic pain relief. *Br. J. Pharmacol.* **2020**, *177*, 580–599. [CrossRef]
77. Han, A.; Xiong, L.; Hao, S.; Yang, Y.; Li, X.; Fang, G.; Liu, J.; Pei, Y.; Wang, S. Highly Bright Self-Assembled Copper Nanoclusters: A Novel Photoluminescent Probe for Sensitive Detection of Histamine. *Anal. Chem.* **2018**, *90*, 9060–9067. [CrossRef]
78. Liu, W.; Chen, J.; Xu, Z. Fluorescent probes for biothiols based on metal complex. *Coord. Chem. Rev.* **2021**, *429*, 213638. [CrossRef]
79. Han, A.; Luo, X.; Hao, S.; Yang, Y.; Chen, J.; Fang, G.; Liu, J.; Wang, S. Synthesis of red photoluminescent nickel doped self-assembled copper nanoclusters and their application in biothiol sensing. *Sens. Actuators B Chem.* **2021**, *349*, 130777. [CrossRef]
80. Gao, X.; Wu, J.; Wu, D. Rational design of the beta-galactosidase from Aspergillus oryzae to improve galactooligosaccharide production. *Food Chem.* **2019**, *286*, 362–367. [CrossRef]
81. Huang, Y.; Feng, H.; Liu, W.; Zhang, S.; Tang, C.; Chen, J.; Qian, Z. Cation-driven luminescent self-assembled dots of copper nanoclusters with aggregation-induced emission for beta-galactosidase activity monitoring. *J. Mater. Chem. B* **2017**, *5*, 5120–5127. [CrossRef] [PubMed]
82. Yuan, J.; Wang, L.; Wang, Y.; Hao, J. Stimuli-Responsive Fluorescent Nanoswitches: Solvent-Induced Emission Enhancement of Copper Nanoclusters. *Chem. Eur. J.* **2020**, *26*, 3545–3554. [CrossRef] [PubMed]
83. Ang, C.W.; Jarrad, A.M.; Cooper, M.A.; Blaskovich, M.A.T. Nitroimidazoles: Molecular Fireworks That Combat a Broad Spectrum of Infectious Diseases. *J. Med. Chem.* **2017**, *60*, 7636–7657. [CrossRef] [PubMed]
84. Du, X.; Yan, B.; Wang, J.; Xi, X.; Wang, Z.; Zang, S. Layer-sliding-driven crystal size and photoluminescence change in a novel SCC-MOF. *ChemComm* **2018**, *54*, 5361–5364. [CrossRef]
85. Dong, X.; Huang, H.; Wang, J.; Li, H.; Zang, S. A Flexible Fluorescent SCC-MOF for Switchable Molecule Identification and Temperature Display. *Chem. Mater.* **2018**, *30*, 2160–2167. [CrossRef]
86. Wang, Y.; Zhang, J.; Wang, Q.; Li, H.; Dong, X.; Wang, S.; Zang, S. Fabrication of silver chalcogenolate cluster hybrid membranes with enhanced structural stability and luminescence efficiency. *ChemComm* **2019**, *55*, 14677–14680. [CrossRef]
87. Ding, H.; Chang, J.; He, F.; Gai, S.; Yang, P. Hydrogen Sulfide: An Emerging Precision Strategy for Gas Therapy. *Adv. Healthc. Mater.* **2022**, *11*, 2101984. [CrossRef]
88. Yan, Y.; Zhang, K.; Yu, H.; Zhu, H.; Sun, M.; Hayat, T.; Alsaedi, A.; Wang, S. Sensitive detection of sulfide based on the self-assembly of fluorescent silver nanoclusters on the surface of silica nanospheres. *Talanta* **2017**, *174*, 387–393. [CrossRef]
89. Li, Z.; Xu, Q. Metal-Nanoparticle-Catalyzed Hydrogen Generation from Formic Acid. *Acc. Chem. Res.* **2017**, *50*, 1449–1458. [CrossRef]
90. Ahmed, R.; Liu, G.; Yousaf, B.; Abbas, Q.; Ullah, H.; Ali, M.U. Recent advances in carbon-based renewable adsorbent for selective carbon dioxide capture and separation-A review. *J. Clean. Prod.* **2020**, *242*, 118409. [CrossRef]
91. Basu, S.; Bhandari, S.; Pan, U.N.; Paul, A.; Chattopadhyay, A. Crystalline nanoscale assembly of gold clusters for reversible storage and sensing of CO_2 via modulation of photoluminescence intermittency. *J. Mater. Chem. C* **2018**, *6*, 8205–8211. [CrossRef]
92. Huang, R.; Wei, Y.; Dong, X.; Wu, X.; Du, C.; Zang, S.; Mak, T.C.W. Hypersensitive dual-function luminescence switching of a silver-chalcogenolate cluster-based metal-organic framework. *Nat. Chem.* **2017**, *9*, 689–697. [CrossRef]
93. Dong, X.; Si, Y.; Yang, J.; Zhang, C.; Han, Z.; Luo, P.; Wang, Z.; Zang, S.; Mak, T.C.W. Ligand engineering to achieve enhanced ratiometric oxygen sensing in a silver cluster-based metal-organic framework. *Nat. Commun.* **2020**, *11*, 3678. [CrossRef] [PubMed]
94. Zhang, W.; Lin, D.; Wang, H.; Li, J.; Nienhaus, G.U.; Su, Z.; Wei, G.; Shang, L. Supramolecular Self-Assembly Bioinspired Synthesis of Luminescent Gold Nanocluster-Embedded Peptide Nanofibers for Temperature Sensing and Cellular Imaging. *Bioconjug. Chem.* **2017**, *28*, 2224–2229. [CrossRef] [PubMed]
95. Wang, C.; Huang, Y.; Lin, H.; Xu, Z.; Wu, J.; Humphrey, M.G.; Zhang, C. Gold nanoclusters based dual-emission hollow TiO_2 microsphere for ratiometric optical thermometry. *RSC Adv.* **2015**, *5*, 61586–61592. [CrossRef]